Astronomy & Astrophysics

Starbursts and black hole masses in X-shaped radio galaxies: Signatures of a merger event?

M. Mezcua[1,2,3], V. H. Chavushyan[4], A. P. Lobanov[1,*], and J. León-Tavares[5]

[1] Max Planck Institute for Radio Astronomy, Auf dem Hügel 69, 53121 Bonn, Germany
e-mail: mmezcua@iac.es
[2] Instituto de Astrofísica de Canarias, vía Láctea S/N, 38200 La Laguna, Tenerife, Spain
[3] Dept. Astrofísica, Universidad de La Laguna (ULL), 38206 La Laguna, Tenerife, Spain
[4] Instituto Nacional de Astrofísica, Óptica y Electrónica, Apdo. Postal 51, 72000 Puebla, México
[5] Aalto University Metsähovi Radio Observatory, Metsähovintie 114, 02540 Kylmälä, Finland

ABSTRACT

We present new spectroscopic identifications of 12 X-shaped radio galaxies and use the spectral data to derive starburst histories and masses of the nuclear supermassive black holes in these galaxies. The observations were done with the 2.1-m telescope of the Observatorio Astronómico Nacional at San Pedro Mártir, México. The new spectroscopic results extend the sample of X-shaped radio galaxies studied with optical spectroscopy. We show that the combined sample of the X-shaped radio galaxies has statistically higher black-hole masses and older episodes of star formation than a control sample of canonical double-lobed radio sources with similar redshifts and luminosities. The data reveal enhanced star-formation activity in the X-shaped sample on the timescales expected in galactic mergers. We discuss the results obtained in the framework of the merger scenario.

Key words. galaxies: kinematics and dynamics – galaxies: formation – galaxies: nuclei – black hole physics

1. Introduction

A significant fraction of the most powerful FRII (Fanaroff & Riley type II; Fanaroff & Riley 1974) radio galaxies exhibit two pairs of misaligned radio lobes associated with the same parent galaxy (Leahy & Williams 1984), giving these galaxies a peculiar X-shaped appearance, which is remarkably different from the "canonical" double-lobed morphology of radio galaxies. Hence, these objects are often branded "winged" or "X-shaped" radio galaxies (Leahy & Williams 1984; Leahy & Parma 1992). A recent merger of two supermassive black holes (SMBHs), where the wings constitute the relic emission of the past radio jets, is one of several scenarios proposed to explain this peculiar radio morphology (e.g., Rottmann 2001; Merritt & Ekers 2002; Komossa 2006; Gergely & Biermann 2009; Hodges-Kluck et al. 2010b; Mezcua et al. 2011). Alternative models employ jet-axis reorientation (e.g., Dennett-Thorpe et al. 2002), two unresolved active galactic nuclei (AGN; Lal & Rao 2007), backflow of material from the main lobes into the wings (e.g., Leahy & Williams 1984; Capetti et al. 2002; Hodges-Kluck et al. 2010a; Landt et al. 2010; Hodges-Kluck & Reynolds 2011), or non-ballistic precession assuming a pre-merger state of the two black holes (BHs; Gong 2008; Gong et al. 2011). The existence of very few X-shaped sources with FRI edge-darkened radio lobes (Saripalli et al. 2008; Saripalli & Subrahmanyan 2009) was initially used as a strong argument against the backflow scenario. However, the presence in most of the FRI X-shaped galaxies of double-double morphologies indicative of a renewal of jet activity, together with an alignment between the main radio axis and the major axis of the host galaxy, led to the proposal of a common formation mechanism for FRI and FRII X-shaped galaxies via

backflows (Saripalli & Subrahmanyan 2009). The required duration of these backflows is, however, too close to the typical radio-source lifetime of 10^8 yr (e.g., Rottmann 2001; Lal & Rao 2007), which again argues against the backflow scenario.

Each of the models mentioned above thus has difficulties in explaining the entire range of the observed properties of the X-shaped radio galaxies (see Gopal-Krishna et al. 2012, for a review). If the observed X-shaped morphology results from a coalescence of a pair of SMBHs, the imprints of the preceding galactic merger should be observed in the X-shaped radio sources in the form of early-type host galaxies (Toomre 1977), statistically higher BH masses, and enhanced star-formation and nuclear activity (e.g., Kauffmann & Haehnelt 2000; Hopkins et al. 2008). It would therefore be relevant to investigate whether BH masses and star-formation activities differ between X-shaped radio galaxies and canonical double-lobed radio sources. We initiated such a study by analyzing the optical spectra of 29 X-shaped sources and 36 radio-loud control sources (cf., Mezcua et al. 2011). The results revealed that all the X-shaped sources analyzed are hosted by early-type galaxies, and that the X-shaped sample has a statistically higher mean BH mass and older bursts of star formation than the control sample of canonical radio galaxies (Mezcua et al. 2011, hereafter M11). A total of 52 X-shaped radio galaxies have been spectroscopically identified so far in several studies (Cheung et al. 2009; Landt et al. 2010), but not all of these observations are suitable for detailed spectral analysis. To increase the statistical significance of our studies, we identified a sample of 13 X-shaped radio sources with bright optical nuclei suitable for optical spectroscopy observations. We present here the results of the spectroscopic observations and discuss them in the context of physical models proposed to explain the nature of the X-shaped radio galaxies.

---

* Visiting Scientist, University of Hamburg/Deutsches Elektronen Synchrotron Forschungszentrum.

The objects selected and the optical observations of the sample are described in Sect. 2. Procedures applied for the analysis of the measurements are explained in Sect. 3. The results and discussion are presented in Sects. 4 and 5, respectively. Throughout the paper, we assume a Λ CDM cosmology with parameters $H_0 = 73$ km s^{-1} Mpc^{-1}, $\Omega_\Lambda = 0.73$, and $\Omega_m = 0.27$.

2. Observations and data reduction

The observed sample comprises 13 X-shaped radio galaxies retrieved from a list of 100 candidates (Cheung 2007). We selected all the objects with bright ($m_R < 19$), optical counterparts for which neither spectroscopic redshifts had been reported nor spectra were available in the Sloan Digital Sky Survey (SDSS), and which were observable during the period of the observations (i.e., across a range of right ascension between 07:00:00 and 17:00:00).

Optical spectroscopy observations of the sample were carried out on 20−23 March 2009 with the 2.1-m telescope of the Observatorio Astronómico Nacional at San Pedro Mártir (OAN-SMP), Baja California, México. The Boller & Chivens spectrograph was tuned to the 4000 Å to 8000 Å range (grating 300 l/mm), with a spectral dispersion of 4.0 ± 0.3 Å/pix, corresponding to 8.0 ± 1.2 Å full width at half maximum (FWHM), derived from the FWHM of different emission lines of the arc-lamp spectrum. The instrumental resolution estimated for each object from the FWHM of the night-sky line at 5575 Å is in the range 9−14 Å. A 2″5 slit oriented along right ascension was used. To calibrate the spectral measurements, the spectrophotometric standard star Feige 34 was observed two times during every night of the observing run. The airmass of the observations ranged between 1.0 and 1.3.

For each target source, two or three exposures were taken, with a typical exposure duration of 1800 s (see Table 1). The data reduction was carried out with the IRAF[1] software following standard procedures. The spectra were bias-subtracted and corrected with dome flat-field frames. Cosmic rays were removed interactively from all images. Arc-lamp (CuHeNeAr) exposures were used for the wavelength calibration. A spline function was fitted to determine the dispersion function (wavelength-to-pixel correspondence). Sky emission lines located at known wavelengths were removed during the calibration in wavelength. The absolute flux-calibration accuracy of the spectra, provided by the standard star calibration, is about 15%. The relative flux-calibration uncertainty, estimated as the difference between the normalized true and estimated flux-calibration curves of the standard star, is <15% for all nights.

3. Analysis of the spectra

The optical spectra were used to identify the most prominent emission/absorption lines, determine the galaxy redshifts, obtain mass estimates for the nuclear SMBH, and reconstruct histories of star-formation activity in the host galaxies.

Since most of the observed spectra of the target objects do not show strong emission lines, we determined the redshift from the Ca II H λ3968 Å and K λ3934 Å, G band λ4302 Å, Mg Ib λ5175 Å, and Na Id λ5896 Å absorption lines.

[1] IRAF is distributed by the National Optical Astronomy Observatories operated by the Association of Universities for Research in Astronomy, Inc. under cooperative agreement with the National Science Foundation.
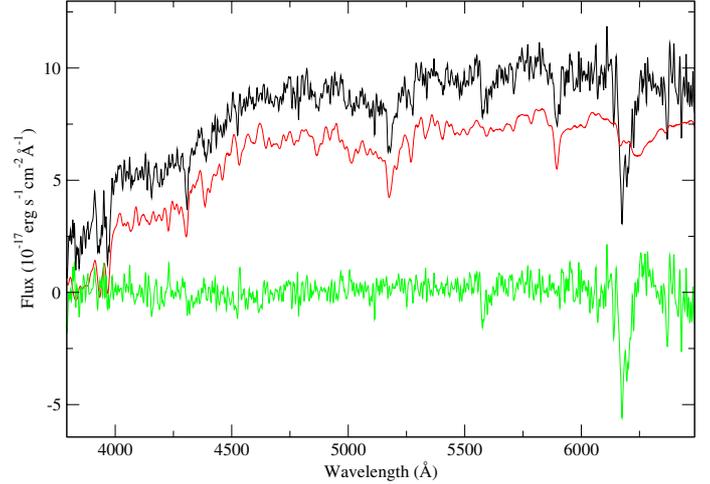
Fig. 1. STARLIGHT fit to the spectrum of the X-shaped radio galaxy J1201-0703. The observed spectrum is shown in black, the modeled in red (for illustration purposes, displaced from the observed spectrum). Residuals obtained after subtraction of the modeled spectrum from the observed one are shown in green.

Table 1. Observation log.

Name	m_R	Obs. date	Exp. time
(1)	(2)	(3)	(4)
J0813+4347	16.1	2009 Mar. 20	2 × 1800
		2009 Mar. 22	2 × 1800
J0838+3253	16.9	2009 Mar. 21	2 × 1800
		2009 Mar. 23	2 × 1800
J0924+4233	17.8	2009 Mar. 23	2 × 1800
J1008+0030	15.8	2009 Mar. 20	2 × 1800
		2009 Mar. 22	2 × 1800
J1055-0707	17.6	2009 Mar. 20	3 × 1800
J1200+6105	18.3	2009 Mar. 23	2 × 1800
J1201-0703	16.4	2009 Mar. 22	2 × 1800
		2009 Mar. 23	2 × 1800
J1258+3227^a	17.0	2009 Mar. 20	2 × 1800
J1351+5559	15.1	2009 Mar. 22	2 × 1800
		2009 Mar. 23	1 × 1800
J1408+0225	18.4	2009 Mar. 22	3 × 1800
J1459+2903	16.5	2009 Mar. 21	2 × 1800
J1537+2648	18.3	2009 Mar. 22	2 × 1800
		2009 Mar. 23	2 × 1800
J1606+0000	15.0	2009 Mar. 21	2 × 1800

Notes. (1) Object name based on J2000.0 coordinates; (2) apparent magnitude R, taken from Cheung (2007); (3) observation date; (4) exposure time, in seconds. $^{(a)}$ Optical misidentification in Cheung et al. (2009). The spectrum of this object corresponds to a K-type star and not a X-shaped radio galaxy.

We used the stellar population synthesis code STARLIGHT (Asari et al. 2007; Cid Fernandes et al. 2004, 2005, 2007; Mateus et al. 2006) to model the observed spectra. The best fit was obtained by constructing a linear combination of simple stellar populations (SSPs) from the stellar library of Bruzual & Charlot (2003) and adding a power-law component representing the AGN continuum emission (see Fig. 1; e.g., León-Tavares et al. 2011).

The STARLIGHT model for the observed spectra yields an estimate of stellar velocity dispersion σ_*, which we corrected by taking into account the spectral resolution of each object, and from which we derived the BH mass using the empirical
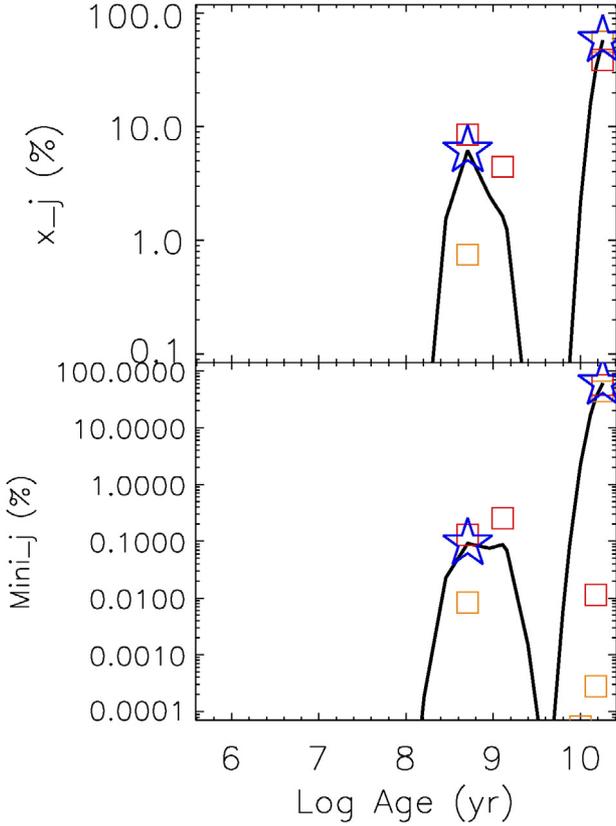
Fig. 2. Age vs. mass fraction (*bottom*) and light fraction (*top*) of the stellar populations synthesized in the fitting of the spectrum of the X-shaped source J1201-0703. The squares correspond to stellar populations with different metallicities (in the color version: orange 1.0 $Z_\odot$ and red 2.5 $Z_\odot$). The solid curve represents Gaussian smoothing of the mass fraction and light fraction distributions. The resulting peaks or bursts of star formation are marked with a star.

$M_{BH} - \sigma_*$ relation (Gebhardt et al. 2000; Tremaine et al. 2002), and the light fraction, mass fraction, age, and metallicity of the stellar populations used in the fit. We used these parameters to derive starburst histories and apply Gaussian smoothing to the individual starburst events in order to determine the epoch of the most recent starburst episode (see Fig. 2). A quality factor Q was derived from the χ^2 of the modeled spectra in order to quantify the reliability of the fit. Fits with $Q > 10$ can be considered reliable (see M11 for details).

We estimated the rest-frame continuum flux at 5100 Å from the SDSS photometry (Wu & Liu 2004). To assess the spectral classification of the X-shaped radio galaxies, we measured the Ca II break ($C_{Ca II}$) of their absorption optical spectrum (Landt et al. 2002) as done in M11.

Finally, we determined the dynamic age (t_a) of the high-surface-brightness (active) radio lobes using θ_a/v_a, where θ_a is the angular size in the FIRST image, converted to linear size assuming that the sources are in the plane of the sky, and v_a is the lobe advance speed. We adopted $v_a \approx 0.1\,c$, as obtained from observations of the aging of the synchrotron radiation spectrum in radio galaxies (e.g., Scheuer 1995; Tingay et al. 1998).

Assuming that the fueling of the low-surface-brightness lobes of the X-shaped sources had stopped after the high-surface ones were activated, the dynamic age of the passive lobes t_p during their active stage can be estimated as

$$t_p = \frac{\theta_p - t_a v_p}{v_a}, \qquad (1)$$

where θ_p is the angular size of the low-surface brightness lobes, converted to linear size assuming that the sources are in the plane of the sky, and v_p is their expansion speed during the inactive stage. We use $v_p = 0.01\,c$ in our calculation.

4. Results

The new data provide the first spectroscopic identifications and redshifts for 8 X-shaped radio galaxies (J1008+0030, J1055-0707, J1200+6105, J1201-0703, J1351+5559, J1408+0225, J1459+2903, and J1537+2648). New spectra were obtained for another 4 X-shaped sources (J0813+4347, J0838+3253, and J0924+4233, spectroscopically identified in the SDSS, Adelman-McCarthy et al. 2007, and for J1606+0000, identified by Best et al. 1999). The difference between our redshifts and the ones obtained previously are $\delta_z < 0.002$. The spectrum of these 12 sources is shown in Fig. 3. With the new identifications, the total number of X-shaped radio galaxies spectroscopically identified is increased to 60. The last object of our sample, J1258+3227, shows the typical stellar lines of a K-type star (G band, Hβ, Mg I, Fe I, and Na I absorption lines; Fig. 4), indicating that there has been a likely misidentification (as also suggested by Cheung et al. 2009). This object is excluded from further analysis. Combined results from the fits to the optical spectra, the BH mass calculations, the epochs of the most recent starburst, and the age estimates for the radio lobes are presented in Table 2. The columns listed are: object name based on J2000.0 coordinates (Col. 1), other common catalog names (Col. 2), stellar velocity dispersion (Col. 3), BH mass derived from σ_* (Col. 4), optical luminosity of the AGN (Col. 5) and of the host galaxy (Col. 6), radio luminosity (Col. 7), dynamic age of the radio lobes (Col. 8), most recent starburst age (Col. 9), the value of Ca II break factor (Col. 10), spectroscopic redshift (Col. 11), and quality factor of the STARLIGHT fit (Col. 12). The total (active + passive lobe) age of the radio emission is given in brackets in Col. 8. The objects J0813+4347, J0838+3253, and J0924+4233 were previously analyzed in M11. We report here their new values of stellar velocity dispersion, BH mass, most recent starburst age, Ca II break factor, spectroscopic redshift, and quality factor (Q) of the STARLIGHT fit derived from the new spectra. The new fits have higher values of Q than in previous analysis and are used for the combined statistical study.

The addition of the new spectroscopical identifications to the X-shaped sample of M11 provides an extended X-shaped sample of 38 sources. This extended sample is considered from now on for the statistical comparison against a control sample consisting of 36 radio-loud sources with redshift $z < 0.3$, and covering the same range of optical and radio luminosities as the X-shaped sample. A control subsample of elliptical radio-loud sources with values of $C_{Ca II} > 0.25$ and that qualify as early-type galaxies according to color-color diagnostics (i.e., location above the *u-r* galaxy type separator in a color-color diagram; Strateva et al. 2001) is also considered for the statistical comparison (selection of both samples is described in detail in M11). The morphological classification based on visual inspection of SDSS images of this subsample of elliptical control sources agrees with the one based on the Ca II break and color-color diagram.

4.1. Luminosity matching

To provide a closer statistical matching between the target and control samples, we used tight radio and optical luminosity matching between the two samples.
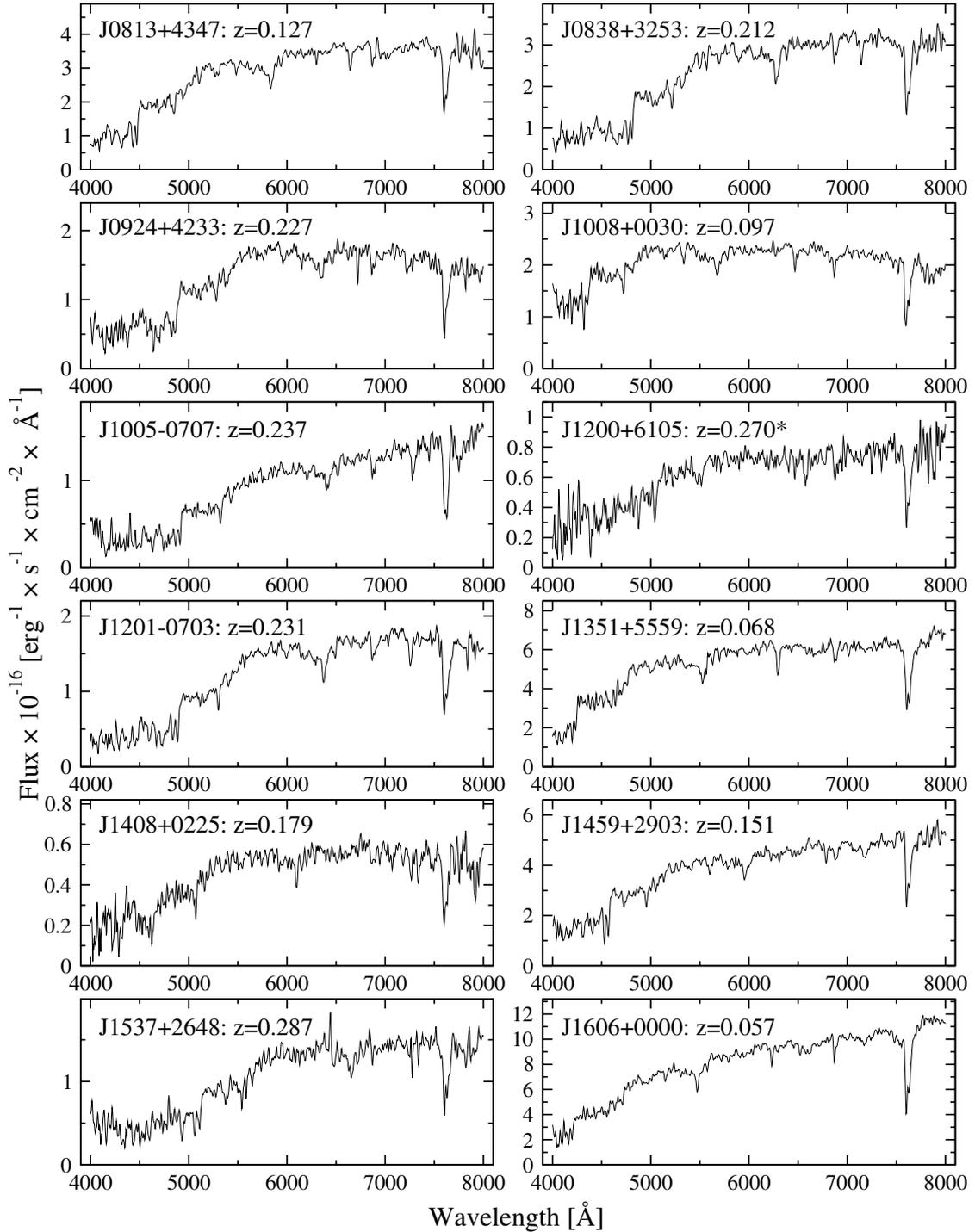
Fig. 3. Optical spectrum and redshift of the targeted X-shaped radio sources. * The noisy spectrum of J1200+6105 results in a higher uncertainty of the redshift determination for this object.

We derived the optical luminosities of all of the 12 X-shaped radio galaxies except for two (J1055-0707 and J1201-0703), whose rest-frame continuum flux at 5100 Å cannot be estimated owing to their lack of SDSS photometry. These sources are excluded from the statistical study. Figure 5 compares the radio and optical luminosities in the combined target and control samples (with the new X-shaped objects marked). All new sources fall in the common range of luminosities $\log \lambda L_{5100\,\text{Å}} \in$ [43.0, 46.0] and $\log \nu L_{1.4\,\text{GHz}} \in$ [39.0, 44.5], defined in M11 as Region 0, and eight of them fall within a tighter range of luminosities called Region 1 (with $\log \lambda L_{5100\,\text{Å}} \in$ [43.5, 44.25]

and $\log \nu L_{1.4\,\text{GHz}} \in$ [40.25, 42.5]; see M11 for further details of the region definition).

The Kolmogorov-Smirnov (KS) test applied to the optical and radio luminosities of the extended X-shaped sample and the control sample in Region 0 gives a probability >5% that the two samples are drawn from the same parent distribution. In Region 1, the KS-test indicates that the probability that the two samples are the same is 87% for the optical luminosity and 19% for the radio luminosity. Therefore, the KS tests suggest that the X-shaped and control sample sources are indistinguishable in terms of optical and radio luminosities within Region 1.
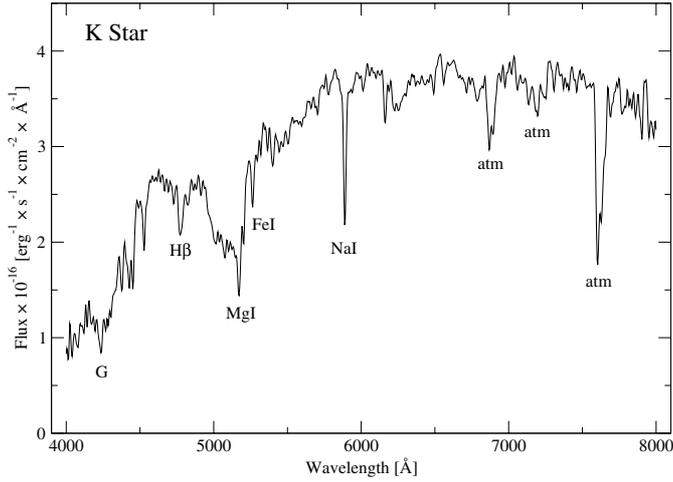
Fig. 4. Spectrum of the optical counterpart of J1258+3227, showing stellar lines typical of a K-type star. This object is excluded from our analysis.
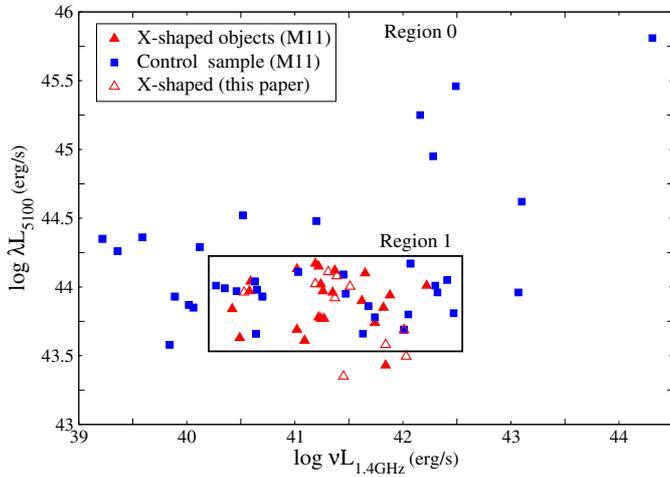

Fig. 5. Optical continuum luminosity versus radio luminosity at 1.4 GHz for the X-shaped sources of M11 (filled triangles), control sources (squares), and the new X-shaped sources analyzed here (empty triangles). A small subregion ("Region 1") marked by a rectangle inside the plot is identified to provide a tighter luminosity match between the X-shaped and control samples (see M11 for details).

4.2. Host type

The new spectra present typical features of early-type galaxies, showing strong metal absorption lines but no optical emission lines, and with values of the Ca II break of $C_{\mathrm{CaII}} \geq 0.3$ in all the sources, and $C_{\mathrm{CaII}} \geq 0.4$ in 10 of them (see Table 2, Col. 10). These values ensure that the galaxy is dominated by the thermal spectrum of the host rather than the non-thermal spectrum of an active nucleus or a relativistic jet. The host galaxy type can be inferred using a color-color diagram, obtained from the SDSS u, g, and r-band photometry. We apply a color-color distinction (Strateva et al. 2001) to identify the type of the host galaxy in the 10 new X-shaped sources considered for the statistical analysis. The combined plot presented in Fig. 6 shows that the new sources also qualify as early-type galaxies.

4.3. Black hole masses

From the individual estimates of the BH mass, we calculated the mean BH mass in the extended X-shaped sample, $\langle M_{\mathrm{BH,X-shaped}}\rangle$,
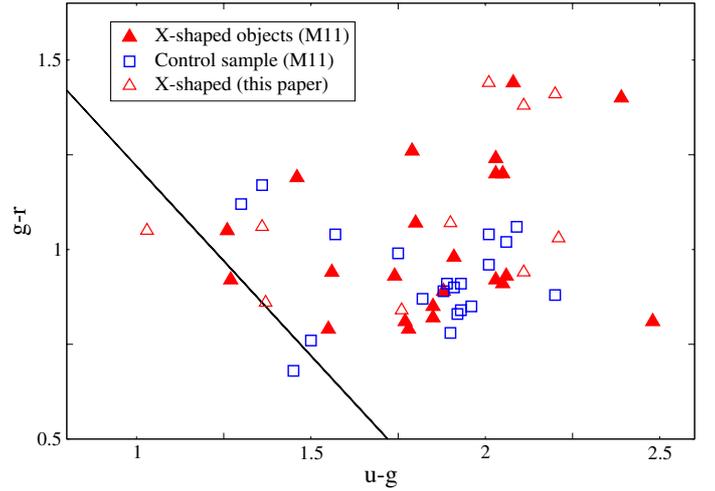

Fig. 6. Color–color diagram ($g - r$ colors versus $u - g$ colors) for the 10 new X-shaped sources analyzed here (empty triangles), the X-shaped sources from M11 (filled triangles), and the control sources from M11 (squares). Black line: $u-r = 2.22$ galaxy type separator from Strateva et al. (2001). Sources situated above this line are classified as early-type galaxies.

and derived its ratio to the mean BH mass in the control samples $r_{\mathrm{xc}} = \langle M_{\mathrm{BH,X-shaped}}\rangle/\langle M_{\mathrm{BH,control}}\rangle$. The resulting ratio is $1.49^{+0.24}_{-0.20}$ for the X-shaped/control samples and $1.13^{+0.20}_{-0.17}$ for the X-shaped/control (ellipticals) samples. These values increase to $1.93^{+0.42}_{-0.34}$ and $1.50^{+0.36}_{-0.29}$, respectively, in the tighter Region 1. The ratios obtained are similar to the ones obtained for the previously published sample of M11, for which $r_{\mathrm{xc}} > 1$ were found in both Regions 0 and 1. The median ratios are $1.03^{+0.29}_{-0.25}$ for the X-shaped/control samples and $1.01^{+0.25}_{-0.21}$ for the X-shaped/control (ellipticals) samples in Region 0, and $1.03^{+0.43}_{-0.36}$ and $1.02^{+0.36}_{-0.30}$, respectively, in the tighter Region 1. While the difference between the mean and the median values of the mass ratios is significant, it should be noted that application of the median is best justified for samples featuring a small number of strong outliers, which is not the case for any of our samples. Furthermore, the KS-test applied to the BH mass distribution of the X-shaped and control sample gives probabilities of 85% and 96% that the two samples differ significantly in Regions 0 and 1, respectively, confirming the difference between BH masses in the two samples expressed by the mean values of the mass.

The differences between the BH masses of the two samples are further illustrated by the distribution of BH masses in Figs. 7, 8. The histograms of the mass distributions for the X-shaped and control samples in Regions 0 and 1 underline the trend of the X-shaped objects having statistically higher BH masses than the control sample. About 85% of the X-shaped sources in Region 0 and 83% in Region 1 have log $M_{\mathrm{BH}} > 8$ $M_{\odot}$. The percentages for the control sample objects are 67% and 55% in Regions 0 and 1, respectively. These results lend further support to the merger scenario in which a BH coalescence could explain the higher BH masses obtained in the X-shaped sample and be the possible origin of the X-shaped morphology.

4.4. Starbursts

Distributions of the ages of the most recent starburst are compared in Fig. 9 for the extended X-shaped sample and the control samples. Both samples present a peak of starburst activity in the range of $10^{6.0}-10^{6.5}$ years. The X-shaped sample notably
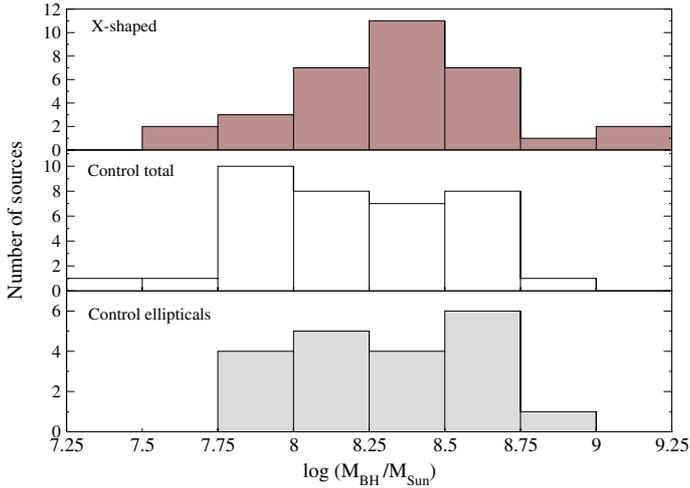
Fig. 7. Histogram of the BH mass in Region 0 for the extended sample of X-shaped sources (*top*), entire sample of control galaxies (*middle*), and control ellipticals (*bottom*).
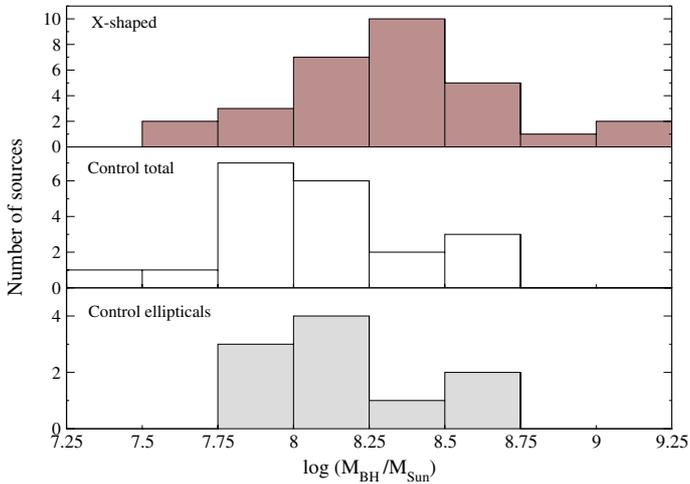

Fig. 8. Histogram of the BH mass in Region 1 for the extended sample of X-shaped sources (*top*), entire sample of control galaxies (*middle*), and control ellipticals (*bottom*).

Fig. 9. Histogram of the ages of the most recent starburst for X-shaped sources (*top*), entire sample of control galaxies (*middle*), and control ellipticals (*bottom*) in Region 0.

Fig. 10. Logarithmic ratios of the dynamic ages of the radio emission to the age of the most recent starburst for Region 0. The top row presents the ages of active lobes in X-shaped objects, while the second row shows the sum of the ages of the active and passive lobes. The two bottom rows show distributions of the age ratios in the entire sample of control galaxies (third row) and the control subsample of ellipticals (fourth row).

exhibits a more prominent spread in the starburst ages, with 50% of the sources having a starburst activity older than 10^8 years. The addition of the new galaxies to the X-shaped sample of M11 not only confirms this trend but also reveals a secondary peak between $10^{9.0}-10^{9.5}$ years in the distribution of starburst ages of the extended X-shaped sample (see Fig. 9). The most recent peak of star formation, which is present in all three samples, could be related to the current jet activity (e.g., Rees 1989; Labiano et al. 2008; Silk & Norman 2009). The secondary peak, which is only present in the extended X-shaped sample, cannot be linked to the active lobes as their oldest dynamic age is $\sim 10^6$ years (see Table 2, Col. 8). This strong starburst activity can only possibly be related to an event that occurred before the active lobes were formed. A delay between a merger-driven starburst and AGN activity is shown in recent studies (e.g., Schawinski et al. 2010; Blecha et al. 2011). This scenario can be tested by comparing the starburst ages to the dynamic ages of the radio lobes for both the X-shaped and control samples. Histograms of the logarithmic ratio of the dynamic age to the most recent starburst age are shown in Fig. 10. The X-shaped sources tend to have older starburst ages than the dynamic ages of the radio lobes, while these
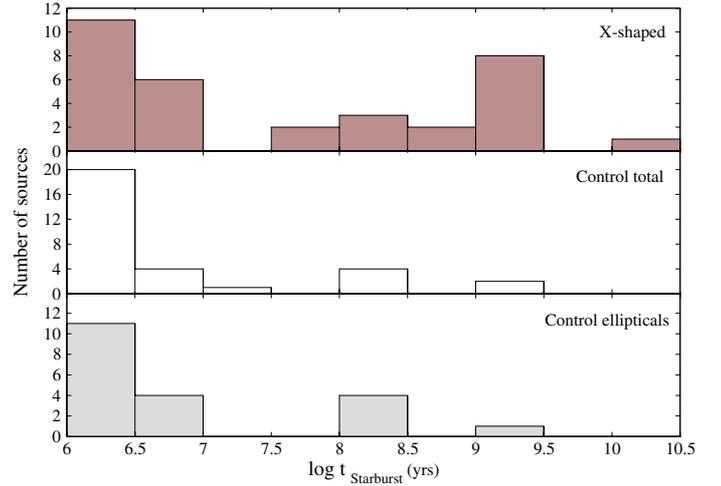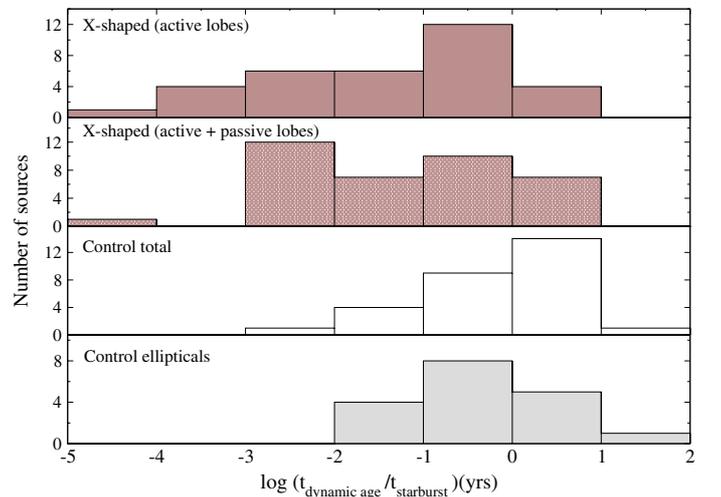
two ages are comparable in the control sample. This trend in the X-shaped sample is observed for both the active lobes alone and the active plus passive lobes (see Fig. 10). The mean logarithmic ratio of the extended X-shaped sample is -1.43 ± 0.23, while that of the control sample is -0.14 ± 0.18. According to the KS-test, the starburst ages of the X-shaped sample and the control sample differ with a probability of 98% in both Regions 0 and 1. Considering the subsample of only control ellipticals, the KS-test gives a somewhat lower probability of 95.5% of the X-shaped objects being different from the control sample.

Since the dynamic ages have been derived from the linear sizes of the radio lobes, we check for differences in the linear size distributions of the X-shaped and control samples. The KS-test finds that the linear size distributions differ with a probability of 87%. This difference is confirmed by the mean values of the distributions, which are (0.22 ± 0.02) Mpc for the X-shaped

Table 2. X-shaped objects.

Name		$\sigma_\star$	log $M_{\rm BH}$	log $\lambda L_{\rm opt}^{\rm agn}$	log $\lambda L_{\rm opt}^{\rm gal}$	log $\nu L_{\rm rad}$	log $t_{\rm a}$ (log $t_{\rm p}$)	log $t_{\rm sb}$	$C_{\rm Ca\,II}$	z	Q
J2000	Other	[km s^{-1}]	[$M_\odot$]	[erg/s]	[erg/s]	[erg/s]	[yr]	[yr]			
(1)	(2)	(3)	(4)	(5)	(6)	(7)	(8)	(9)	(10)	(11)	(12)
J0813+4347		274 ± 83	8.7 ± 0.5	–^{a}	44.11	41.31	6.29 (6.49)	9.11	0.45^c	0.127	259
J0838+3253		237 ± 79	8.4 ± 0.6	–^{a}	43.92	41.37	6.59 (6.76)	8.71	0.50	0.212	88
J0924+4233		266 ± 102	8.6 ± 0.7	–^{a}	43.58	41.84	6.54 (6.77)	9.11	0.42^c	0.227	117
J1008+0030		340 ± 41	9.1 ± 0.2	41.73 ± 1.37	44.02	41.19	5.61 (5.93)	6.00	0.32	0.097	709
J1055−0707		261 ± 46	8.6 ± 0.3	–^{a}	–^{b}	42.24	6.14 (6.30)	7.40	0.47	0.237	72
J1200+6105		165 ± 74	7.8 ± 0.8	43.27 ± 0.20	43.69	42.01	6.08 (6.31)	6.70	0.29	0.270	115
J1201−0703		303 ± 43	8.9 ± 0.2	–^{a}	–^{b}	41.71	5.94 (6.25)	8.71	0.50	0.231	149
J1351+5559		228 ± 78	8.4 ± 0.6	–^{a}	43.96	40.53	5.42 (5.71)	7.00	0.49	0.068	116
J1408+0225		266 ± 53	8.6 ± 0.3	41.53 ± 1.24	43.35	41.45	5.67 (6.01)	10.26	0.39	0.179	313
J1459+2903		153 ± 77	7.7 ± 0.9	41.97 ± 4.57	44.00	41.51	5.98 (6.12)	6.94	0.38	0.151	142
J1537+2648		219 ± 42	8.3 ± 0.3	–^{a}	43.49	42.03	6.05 (6.33)	9.11	0.40	0.287	33
J1606+0000	4C+00.58	227 ± 37	8.3 ± 0.3	42.84 ± 0.27	44.08	41.39	5.50 (5.71)	6.00	0.41^c	0.057	51

Notes. (1) Object name based on J2000.0 coordinates; (2) other common catalog names; (3) stellar velocity dispersion obtained from STARLIGHT; (4) black hole mass obtained from σ_*; (5) 5100 Å continuum luminosity from STARLIGHT; (6) 5100 Å continuum luminosity from SDSS photometry; (7) 1.4 GHz radio luminosity; (8) dynamic age of the active (active+passive) lobes; (9) age of the most recent starburst; (10) value of Ca II break factor; (11) spectroscopic redshift; (12) quality factor. $^{(a)}$ STARLIGHT could not fit the continuum luminosity; $^{(b)}$ no SDSS photometry available; $^{(c)}$ values of Ca II break from Landt et al. (2010).

sample and (0.5 ± 0.2) Mpc for the control sample. The median values are 0.18 Mpc and 0.3 Mpc, respectively. We also study a possible dependence of the linear size with the BH mass and starburst age, but no dependences are found for any of the two samples.

5. Discussion

The origin of the X-shaped morphology in X-shaped radio galaxies is a matter of ongoing debate. Some recent studies in the X-rays (Hodges-Kluck et al. 2010b) and optical (Mezcua et al. 2011) bands and some theoretical models (Gong et al. 2011) favor a recent merger of two SMBHs as the most plausible scenario. Other studies (Hodges-Kluck et al. 2010a; Landt et al. 2010) propose a backflow from the active lobes into the wings to explain the peculiar morphology of X-shaped radio galaxies.

In this paper, we have presented the largest statistical study to date of the BH mass and starburst activity in X-shaped radio sources. The properties of a sample of 38 X-shaped radio galaxies have been compared to those of a control sample of 36 radio-loud active nuclei, by applying stringent luminosity and color criteria to provide the closest match between the two samples. The results suggest that a galactic merger is a more likely explanation of the origin of X-shaped sources. The merger hypothesis is further supported by the finding that all of the X-shaped objects studied are hosted by early-type galaxies, which are expected to have undergone at least one major merger event over the course of their evolution (Toomre 1977).

Histograms of the BH mass distribution for the X-shaped and control samples show that X-shaped radio galaxies tend to have higher $M_{\rm BH}$ than the control sample. The ratio of the mean $M_{\rm BH}$ for the two samples confirms the trend observed, with the X-shaped sample having a mean BH mass that is $1.93^{+0.42}_{-0.34}$ times higher than the one of the control sample in a tight common range of radio and optical luminosities. The higher average BH mass in the galaxies hosting the X-shaped radio sources may result from a major merger event and the consequent coalescence of the two central black holes, which could be the origin of the winged morphology observed in the radio maps.

The occurrence of a merger event in the X-shaped radio galaxies should be reflected in their starburst histories. The age of the most recent burst of star formation and the dynamic age of the radio lobes was thus studied for both the X-shaped and the control samples. The most recent episodes of starburst activity were found to be statistically older in the X-shaped sample than those found for the control sample, with 50% of the X-shaped sources having starburst ages older than 10^8 years. In the X-shaped sources, the most recent starburst occurred before the active lobes were formed. Of particular interest is the peak observed in the distribution of the most recent starburst ages of the X-shaped sample at ages of 10^9–$10^{9.5}$ years (1−3 Gyr). This peak suggests that there has been enhanced star formation due to a merger event, which implies a time delay of 1−3 Gyr between the peak of starburst activity and the end of the merger. This timescale agrees with the time delay of ∼2 Gyr found by hydrodynamical simulations of galaxy mergers (Lotz et al. 2008), and with the timescales of 0.5−2 Gyr found observationally for individual objects (e.g., Tadhunter et al. 2005; Emonts et al. 2006). On the other hand, the jet dynamic age of 10^6 yrs derived for the X-shaped sources also agrees with the time delay between the merger event and the onset of the radio-AGN triggered activity found by other studies to be 10^6 years (e.g., Emonts et al. 2006). These results assume a jet advance speed of $0.1c$. Estimates of the lobe advance speed based on synchrotron aging studies can reach $0.2c$ for the most powerful radio galaxies, while the study of three samples of very powerful radio sources yielded estimates below $0.1c$ (with a poor statistical significance; i.e., Scheuer 1995). The use of an advance speed as low as $0.01c$ in our calculations would increase the dynamic age of the active lobes by an order of magnitude. However, this would not affect the results derived from the ratio of dynamic to starburst ages, which would still indicate that the most recent starburst activity occurred before the active lobe formation. This result is also essentially unchanged when an advance speed of $0.2c$ is used.

All the results obtained in our study strengthen the hypothesis that X-shaped radio galaxies were formed by mergers. More detailed studies of star formation and gas kinematics in these objects will yield stronger constraints of this scenario.

References

Adelman-McCarthy, J. K., Agüeros, M. A., Allam, S. S., et al. 2007, ApJS, 172, 634

Asari, N. V., Cid Fernandes, R., Stasińska, G., et al. 2007, MNRAS, 381, 263

Best, P. N., Röttgering, H. J. A., & Lehnert, M. D. 1999, MNRAS, 310, 223

Blecha, L., Cox, T. J., Loeb, A., & Hernquist, L. 2011, MNRAS, 412, 2154

Bruzual, G., & Charlot, S. 2003, MNRAS, 344, 1000

Capetti, A., Zamfir, S., Rossi, P., et al. 2002, A&A, 394, 39

Cheung, C. C. 2007, AJ, 133, 2097

Cheung, C. C., Healey, S. E., Landt, H., Verdoes Kleijn, G., & Jordán, A. 2009, ApJS, 181, 548

Cid Fernandes, R., Gu, Q., Melnick, J., et al. 2004, MNRAS, 355, 273

Cid Fernandes, R., Mateus, A., Sodré, L., Stasińska, G., & Gomes, J. M. 2005, MNRAS, 358, 363

Cid Fernandes, R., Asari, N. V., Sodré, L., et al. 2007, MNRAS, 375, L16

Dennett-Thorpe, J., Scheuer, P. A. G., Laing, R. A., et al. 2002, MNRAS, 330, 609

Emonts, B. H. C., Morganti, R., Tadhunter, C. N., et al. 2006, A&A, 454, 125

Fanaroff, B. L., & Riley, J. M. 1974, MNRAS, 167, 31

Gebhardt, K., Bender, R., Bower, G., et al. 2000, ApJ, 539, L13

Gergely, L. Á., & Biermann, P. L. 2009, ApJ, 697, 1621

Gong, B. 2008, MNRAS, 389, 315

Gong, B. P., Li, Y. P., & Zhang, H. C. 2011, ApJ, 734, L32

Gopal-Krishna, Biermann, P. L., Gergely, L. Á., & Wiita, P. J. 2012, Res. Astron. Astrophys., 12, 127

Hodges-Kluck, E. J., & Reynolds, C. S. 2011, ApJ, 733, 58

Hodges-Kluck, E. J., Reynolds, C. S., Cheung, C. C., & Miller, M. C. 2010a, ApJ, 710, 1205

Hodges-Kluck, E. J., Reynolds, C. S., Miller, M. C., & Cheung, C. C. 2010b, ApJ, 717, L37

Hopkins, P. F., Hernquist, L., Cox, T. J., & Kereš, D. 2008, ApJS, 175, 356

Kauffmann, G., & Haehnelt, M. 2000, MNRAS, 311, 576

Komossa, S. 2006, Mem. Soc. Astron. It., 77, 733

Labiano, A., O'Dea, C. P., Barthel, P. D., de Vries, W. H., & Baum, S. A. 2008, A&A, 477, 491

Lal, D. V., & Rao, A. P. 2007, MNRAS, 374, 1085

Landt, H., Padovani, P., & Giommi, P. 2002, MNRAS, 336, 945

Landt, H., Cheung, C. C., & Healey, S. E. 2010, MNRAS, 408, 1103

Leahy, J. P., & Parma, P. 1992, in Extragalactic Radio Sources. From Beams to Jets, eds. J. Roland, H. Sol, & G. Pelletier, 307

Leahy, J. P., & Williams, A. G. 1984, MNRAS, 210, 929

León-Tavares, J., Valtaoja, E., Chavushyan, V. H., et al. 2011, MNRAS, 411, 1127

Lotz, J. M., Jonsson, P., Cox, T. J., & Primack, J. R. 2008, MNRAS, 391, 1137

Mateus, A., Sodré, L., Cid Fernandes, R., et al. 2006, MNRAS, 370, 721

Merritt, D., & Ekers, R. D. 2002, Science, 297, 1310

Mezcua, M., Lobanov, A. P., Chavushyan, V. H., & León-Tavares, J. 2011, A&A, 527, A38

Rees, M. J. 1989, MNRAS, 239, 1

Rottmann, H. 2001, Ph.D. Thesis, Univ. Bonn

Saripalli, L., & Subrahmanyan, R. 2009, ApJ, 695, 156

Saripalli, L., Subrahmanyan, R., Laskar, T., & Koekemoer, A. 2008 [arXiv:0806.3518]

Schawinski, K., Dowlin, N., Thomas, D., Urry, C. M., & Edmondson, E. 2010, ApJ, 714, L108

Scheuer, P. A. G. 1995, MNRAS, 277, 331

Silk, J., & Norman, C. 2009, ApJ, 700, 262

Strateva, I., Ivezić, Ž., Knapp, G. R., et al. 2001, AJ, 122, 1861

Tadhunter, C., Robinson, T. G., González Delgado, R. M., Wills, K., & Morganti, R. 2005, MNRAS, 356, 480

Tingay, S. J., Jauncey, D. L., Reynolds, J. E., et al. 1998, AJ, 115, 960

Toomre, A. 1977, in Evolution of Galaxies and Stellar Populations, eds. B. M. Tinsley, & R. B. Larson, 401

Tremaine, S., Gebhardt, K., Bender, R., et al. 2002, ApJ, 574, 740

Wu, X., & Liu, F. K. 2004, ApJ, 614, 91